

Nanoscale

Accepted Manuscript



This is an *Accepted Manuscript*, which has been through the Royal Society of Chemistry peer review process and has been accepted for publication.

Accepted Manuscripts are published online shortly after acceptance, before technical editing, formatting and proof reading. Using this free service, authors can make their results available to the community, in citable form, before we publish the edited article. We will replace this *Accepted Manuscript* with the edited and formatted *Advance Article* as soon as it is available.

You can find more information about *Accepted Manuscripts* in the [Information for Authors](#).

Please note that technical editing may introduce minor changes to the text and/or graphics, which may alter content. The journal's standard [Terms & Conditions](#) and the [Ethical guidelines](#) still apply. In no event shall the Royal Society of Chemistry be held responsible for any errors or omissions in this *Accepted Manuscript* or any consequences arising from the use of any information it contains.

ARTICLE

Encapsulation of α -Fe₂O₃ Nanoparticles in Graphitic Carbon Microspheres as High-Performance Anode Materials for Lithium-Ion Batteries†

Cite this: DOI: 10.1039/x0xx00000x

Hongwei Zhang,^a Xiaoran Sun,^a Xiaodan Huang,^a and Liang Zhou^{*a}

Received 00th January 2012,

Accepted 00th January 2012

DOI: 10.1039/x0xx00000x

www.rsc.org/

A novel "spray drying-carbonization-oxidation" strategy has been developed for the fabrication of α -Fe₂O₃-graphitic carbon (α -Fe₂O₃@GC) composite microspheres, in which, α -Fe₂O₃ nanoparticles with sizes of 30–50 nm are well-encapsulated by onion-like graphitic carbon shells with a thickness of 5–10 nm. In the constructed composite, the α -Fe₂O₃ nanoparticles act as the primary active material, providing high capacity. Meanwhile, the graphitic carbon shells serve as the secondary active component, structural stabilizer, interfacial stabilizer, and electron-highway. As a result, the synthesized α -Fe₂O₃@GC nanocomposite exhibits superior lithium-ion battery performance with high reversible capacity (898 mA h g⁻¹ at 400 mA g⁻¹), outstanding rate capability, and excellent cycling stability. Our product, in terms of the facile and scalable preparation process and excellent electrochemical performance, demonstrates its great potential as a high-performance anode material for lithium-ion batteries.

Introduction

Lithium-ion batteries (LIBs) have been widely employed in portable electronic devices. They have also been identified as the power sources of choice for upcoming hybrid, plug-in hybrid, and all electric vehicles (EVs), which require high energy and power density, long calendar life, and high safety.^{1,2} Graphite, the most popular anode material in current commercialized LIBs, is limited by its low theoretical capacity (372 mA h g⁻¹) and safety. Stimulated by the urgent demand of high-performance anode materials, transition metal oxides (TMOs) have been subject to extensive research due to their high theoretical capacity.^{3,4} Among the TMOs, hematite (α -Fe₂O₃) has attracted much attention because of its non-toxicity, abundance in the earth's crust, and high theoretical capacity (1007 mA h g⁻¹).⁵ Unfortunately, the practical application of α -Fe₂O₃ in LIBs has thus far been hindered by the large volume expansion during lithiation and low electrical conductivity, which result in fast capacity decay and poor rate performance.

To circumvent the above-mentioned problems, two promising strategies have been developed. The first approach, known as nanostructuring, relies on the fabrication of unique nanostructures to shorten the lithium ion diffusion length and alleviate the mechanical strain generated from repeated volume expansion/contraction. In this context, various α -Fe₂O₃ nanostructures, such as nanotubes,⁵⁻⁸ nanorods,⁹⁻¹² nanosheets,¹³ porous materials,^{14,15} and hollow structures,¹⁶⁻²⁰ have been designed and utilized in LIBs. The second approach, so-called nanocompositing, introduces a second component, such as carbon or conductive polymer, to improve the structural stability and conductivity of the active material.²¹⁻²⁷ As an example, α -Fe₂O₃-reduced graphene oxide (Fe₂O₃-RGO)

composite shows much improved cycling stability than bare α -Fe₂O₃ nanoparticles.^{23,24} As another example, α -Fe₂O₃-carbon nanotube (Fe₂O₃-CNT) hybrids exhibit not only better cycling stability but also better rate capability than pristine α -Fe₂O₃.²⁵⁻²⁷

Graphitic carbon (GC) has been known for its superior conductivity, thermal stability, and chemical resistance to amorphous carbon.^{28,29} When applied as the anode material for LIBs, it shows not only higher reversible capacity but also better rate performance than commercialized graphite.^{30,31} It is hypothesized that the Fe₂O₃-GC nanocomposite would integrate the advantages of both Fe₂O₃ (high capacity) and GC (high rate capability and good cyclability). Nevertheless, the preparation of Fe₂O₃-GC nanocomposite has achieved limited success. The challenge for the preparation of Fe₂O₃-GC lies in the fact that graphitic carbon is usually obtained at extremely high carbonization temperatures in inert atmosphere (> 2000 °C);³¹ while the Fe₂O₃ can be reduced to metallic Fe or Fe₃C under similar conditions.

Herein, a novel "spray drying-carbonization-oxidation" strategy has been developed for the fabrication of α -Fe₂O₃@GC nanocomposite, in which the α -Fe₂O₃ nanoparticles are well encapsulated by onion-like graphitic carbon shells. In this novel composite, the α -Fe₂O₃ nanoparticles act as the primary active material, providing high capacity. The graphitic carbon shells serve as i) the secondary active component contributing to the total capacity, ii) the structural stabilizer buffering the large volume expansion of α -Fe₂O₃ nanoparticles, iii) the interfacial stabilizer avoiding the direct exposure of α -Fe₂O₃ nanoparticles to the electrolyte, and iv) the electron-highway making the whole composite highly conductive. When applied as an anode material in LIBs, the synthesized α -Fe₂O₃@GC manifest a high

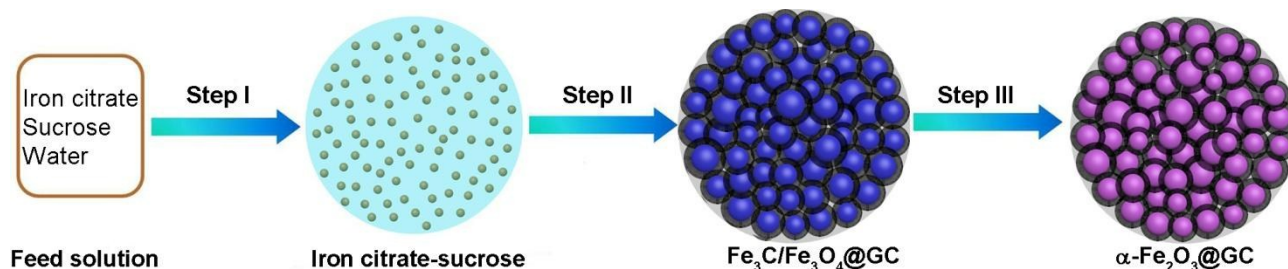


Fig. 1 Schematic illustration for the synthesis of $\alpha\text{-Fe}_2\text{O}_3\text{@GC}$ nanocomposite. Step I: spray drying, Step II: carbonization at 700 °C in N₂, and Step III: oxidation at 350 °C in air.

reversible capacity of 898 mA h g⁻¹ with excellent cycling stability and rate capability.

Experimental

Synthesis

The $\alpha\text{-Fe}_2\text{O}_3\text{@GC}$ nanocomposite was synthesized by a "spray drying-carbonization-oxidation" strategy using iron (III) citrate and sucrose as raw materials. Briefly, iron citrate (10 mmol) and sucrose (10 mmol) were dissolved in water (100 mL) to obtain a light yellow solution. The solution was then spray dried in a Buchi mini spray drier B-290 with nitrogen as the drying gas. The instrument parameter settings were as following: inlet temperature of 220 °C, aspirator rate of 100 %, rotameter setting of 60 mm, and pump rate of 5 % (~1.5 mL min⁻¹). The spray dried product (iron citrate-sucrose composite) was then carbonized at 700 °C for 5 hours in nitrogen. The carbonized sample was then re-oxidized in air at 350 °C for another 5 hours to obtain the $\alpha\text{-Fe}_2\text{O}_3\text{@GC}$ nanocomposite. Pure graphitic carbon microspheres were obtained by eliminating $\alpha\text{-Fe}_2\text{O}_3$ from the $\alpha\text{-Fe}_2\text{O}_3\text{@GC}$ using 2M HCl. Pristine $\alpha\text{-Fe}_2\text{O}_3$ nanoparticles were prepared according to our previous work.²⁴

Materials characterizations

The morphology of the products was investigated by field emission scanning electron microscope (FESEM, JEOL 7001F) at 10 kV and transmission electron microscope (TEM, JEOL 2100) at 200 kV. X-ray diffraction (XRD) patterns were recorded on a Rigaku Miniflex X-ray Diffractometer with Co K α radiation ($\lambda=0.179$ nm). X-ray photoelectron spectra (XPS) were recorded on a Kratos Axis ULTRA X-ray photoelectron spectrometer. Thermo gravimetric analysis (TGA) was performed on a TGA/DSC1 STAR^o System in air flow (25–800 °C, 5 °C min⁻¹).

Electrochemical measurements

The electrochemical measurements were carried out on a MTI 8 Channels Battery Analyzer at room temperature with lithium chips as both the counter electrode and reference electrode. The working electrode was prepared by casting a slurry containing active material (80 wt%), conductive acetylene black (10 wt%), and polyvinylidene fluoride (PVDF) binder (10 wt%) onto a Cu foil. Afterwards, the electrode was dried in a vacuum oven at 115 °C overnight and punched into small disks with a diameter of 13 mm. The electrolyte is composed of 1 M LiPF₆ in a mixture of ethylene carbonate, dimethyl carbonate, and diethyl carbonate (1:1:1 in volume). Swagelok-type cells were

fabricated in an Ar-filled glovebox with moisture and oxygen concentrations below 0.1 ppm. Cyclic voltammogram (CV) measurements were performed on a Solartron 1480 MultiStat instrument a scan rate of 0.1 mV s⁻¹ between 0.001 V and 3.0 V. The capacity was calculated based on the mass of $\alpha\text{-Fe}_2\text{O}_3\text{@GC}$ in the electrode. After cycling, the cell was disassembled and the electrode was dispersed in acetone/ethanol by sonication and washed with acetone/ethanol for three times.

Results and Discussion

The $\alpha\text{-Fe}_2\text{O}_3\text{@GC}$ nanocomposite was synthesized by a facile, low-cost, and scalable "spray drying-carbonization-oxidation" method as schematically illustrated in Fig. 1. In step I, iron citrate-sucrose composite microspheres were obtained by spray drying an aqueous solution of iron citrate and sucrose, which is similar to the preparation of iron nitrate-sucrose microspheres in synthesizing $\alpha\text{-Fe}_2\text{O}_3$ multi-shelled hollow spheres.¹⁸ In step II, the iron citrate-sucrose microspheres were carbonized at 700 °C under inert atmosphere. Multistep and complex processes took place in step II, mainly involving 1) the decomposition of iron citrate into iron oxides; 2) the decomposition of organic species into amorphous carbon; 3) the reduction of iron oxides to metallic Fe and/or Fe₃C; and 4) the formation of graphitic carbon around the *in situ* generated Fe/Fe₃C nanoparticles through dissolution of amorphous carbon into Fe/Fe₃C followed by the precipitation of graphitic carbon,³²⁻³⁴ which led to the formation of Fe₃C/Fe₃O₄@GC (Fig. S1). In step III, the Fe₃C/Fe₃O₄@GC was oxidized at 350 °C in air. The Fe₃C and Fe₃O₄ were converted into $\alpha\text{-Fe}_2\text{O}_3$, while the graphitic carbon shells survived the oxidation due to their high resistance to oxidation, leading to the formation of $\alpha\text{-Fe}_2\text{O}_3\text{@GC}$ encapsulation structure. The graphitic carbon cannot be formed at carbonization temperatures lower than 700 °C. As a result, only pure $\alpha\text{-Fe}_2\text{O}_3$ was obtained after oxidizing (Fig. S2) when a lower carbonization temperature of 500 °C was applied in step II.

The crystalline structure of $\alpha\text{-Fe}_2\text{O}_3\text{@GC}$ was characterized by XRD (Fig. 2a). The major peaks with high intensity can be

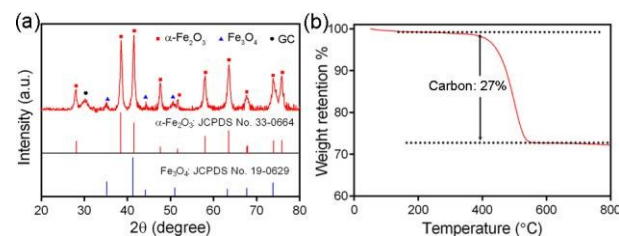


Fig. 2 XRD pattern (a) and TGA thermogram (b) of $\alpha\text{-Fe}_2\text{O}_3\text{@GC}$.

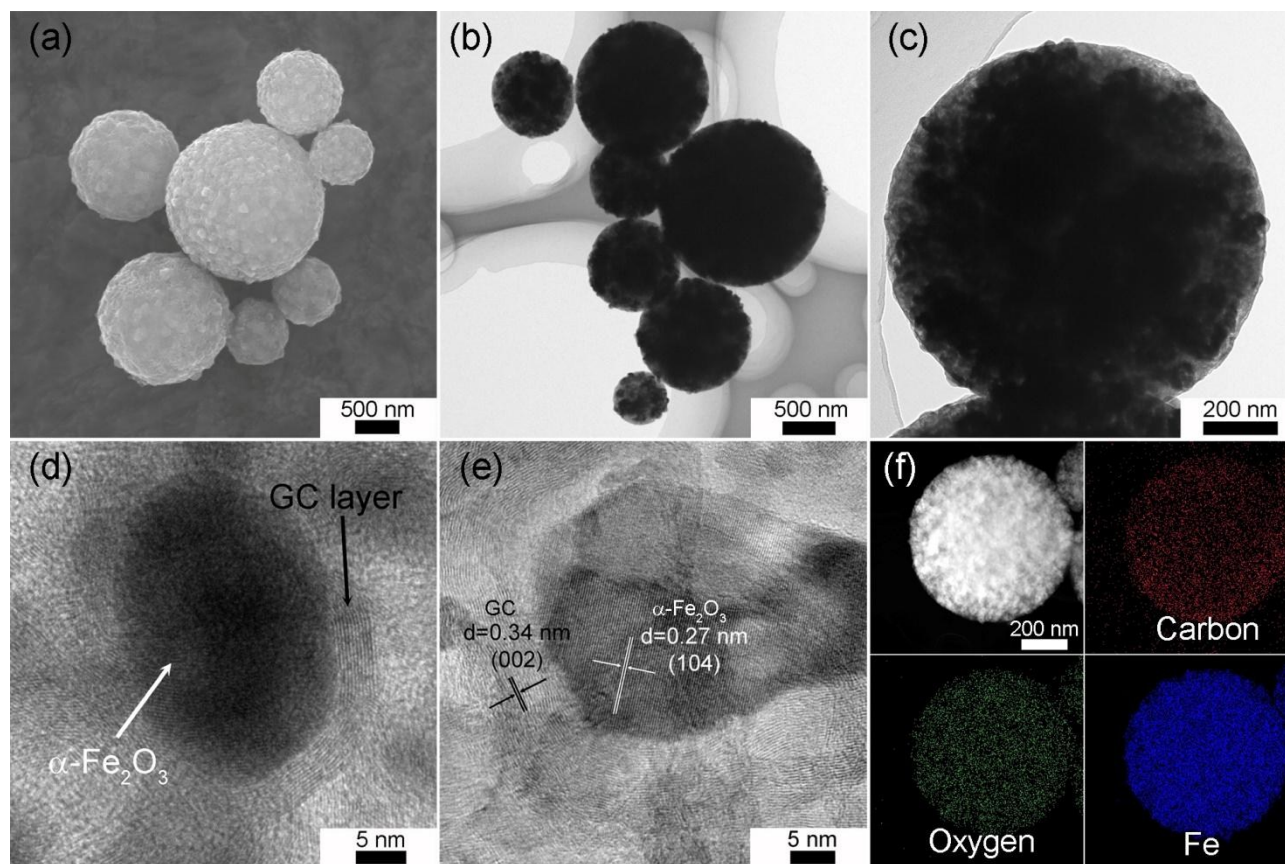


Fig. 3 SEM (a), TEM (b, c), high-resolution TEM (d, e), and elemental mapping (f) of α -Fe₂O₃@GC.

assigned to α -Fe₂O₃ (hematite, JCPDS No. 33-0664); only very weak diffraction peaks from Fe₃O₄ (magnetite, JCPDS No. 19-0629) are observed. The broad peak located at 30.3° originates from the (002) diffraction peak of graphitic carbon. By applying the Scherer Equation to the diffraction peaks, the crystallite size of α -Fe₂O₃ is determined to be 20.0 nm; while the thickness of graphitic carbon is calculated to be 8.2 nm.

The carbon content of α -Fe₂O₃@GC was determined by TGA (Fig. 2b). Usually, the combustion of amorphous carbon in air takes place below 430 °C.³⁵ In our case, a dramatic weight loss is observed between 400 to 550 °C, suggesting the higher stability of graphitic carbon. The high resistance of graphitic carbon to oxidation enables the successful synthesis of α -Fe₂O₃@GC by oxidizing the Fe₃C/Fe₃O₄@GC at 350 °C in air. The weight percentage of carbon is determined to be 27 wt%.

The structure and morphology of α -Fe₂O₃@GC was investigated by SEM and TEM. As shown in Fig. 3a–3c, the α -Fe₂O₃@GC shows microspherical morphology with sizes ranging from several hundred nanometers to two microns. According to the literatures, such microspherical morphology not only provides high tap density but also better fits the current slurry coating manufacturing process for electrodes.³⁶ The α -Fe₂O₃ nanoparticles are well embedded in the graphitic carbon matrix, resulting in a relatively smooth surface (Fig. 3a–3c). This conclusion is further supported by the XPS result (Fig. S3), where only very weak signals of Fe can be detected. A typical α -Fe₂O₃ nanoparticle@graphitic carbon encapsulation structure is presented in Fig. 3d. An onion-like graphitic carbon shell with a thickness of 5–10 nm surrounding the Fe₂O₃ nanoparticulate core with a size of 30–50 nm can be clearly

observed. Well-resolved lattice fringes with a spacing of 0.27 nm from the core and an interplanar spacing of 0.34 nm from the shell can be clearly distinguished (Fig. 3e), which corresponds to the (104) interplanar distance of α -Fe₂O₃ and the (002) interplanar distance of graphitic carbon, respectively. Energy dispersive X-ray spectroscopy elemental mapping results (Fig. 3f) show that carbon, oxygen and iron are homogeneously distributed throughout the composite.

The electrochemical performance of α -Fe₂O₃@GC was then examined in an active material/Li half cell configuration. Fig. S4 shows the CV curves of α -Fe₂O₃@GC. The relatively broad peak at 0.5 V from the first cathodic scanning is corresponding to the reduction of α -Fe₂O₃ to metallic Fe and the formation of solid electrolyte interphase (SEI) layer on the electrode surface. The peak located at 2.0 V in the following anodic process can be ascribed to the oxidation of metallic Fe to Fe³⁺. The curves overlap well after two cycles, indicating the good cycling stability of α -Fe₂O₃@GC.

Fig. 4a presents the representative charge-discharge profiles of α -Fe₂O₃@GC at a current density of 400 mA g⁻¹ between 0.01 and 3.0 V. The composite delivers an initial discharge capacity of 1363 mA h g⁻¹; in the subsequent charge process, a charge capacity of 898 mA h g⁻¹ is achieved, leading to a Coulombic efficiency of 66 %. The irreversible capacity loss (467 mA h g⁻¹) in the first discharge-charge process can be attributed to the inevitable decomposition of electrolyte and formation of SEI film on the surface of the electrode, which is commonly observed in transition metal oxide based anode materials.^{9, 35, 37-39} To investigate the effect of graphitic carbon on the irreversible capacity loss in the first cycle, the

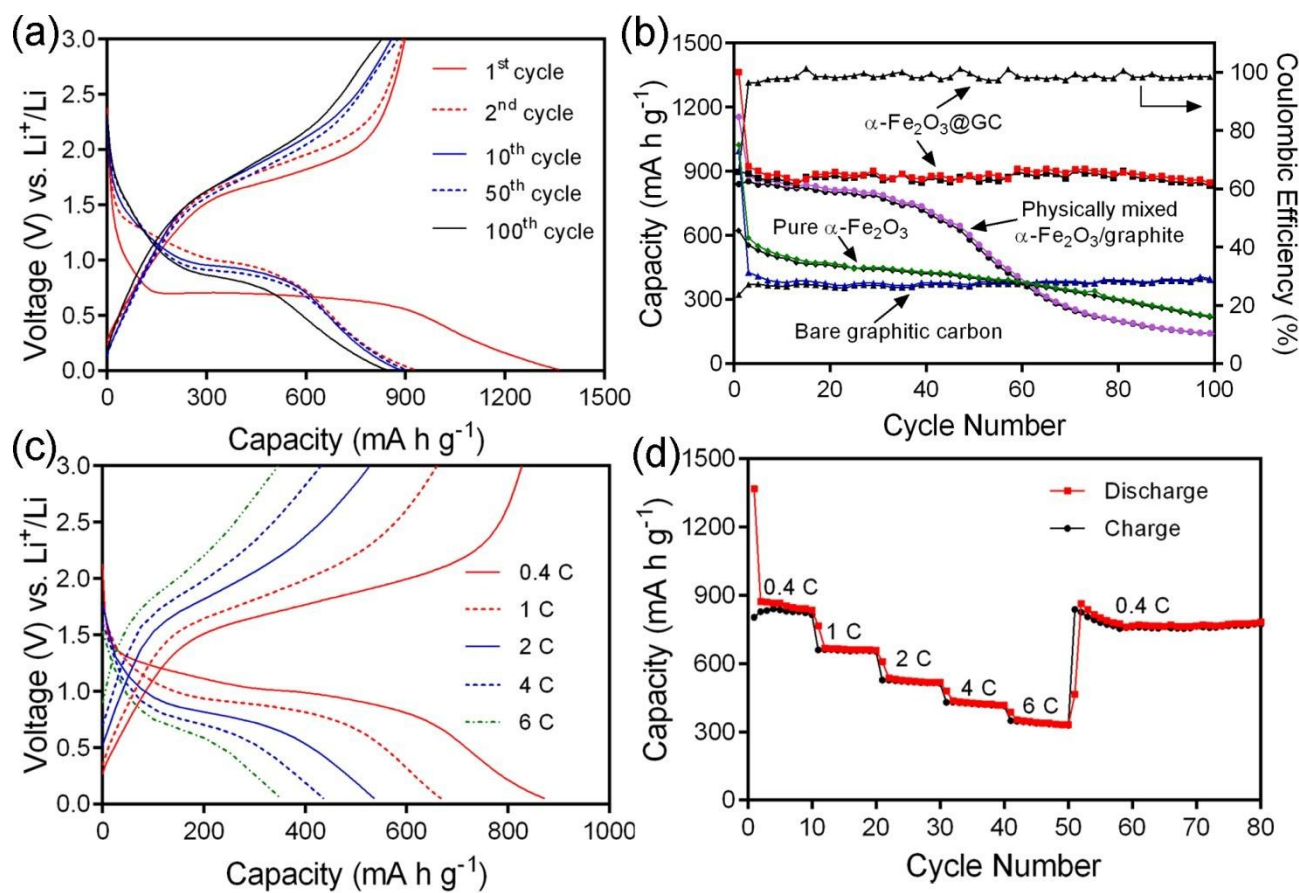


Fig. 4 Representative charge-discharge profiles of $\alpha\text{-Fe}_2\text{O}_3\text{@GC}$ at 400 mA g^{-1} (a), cycling performance of pristine $\alpha\text{-Fe}_2\text{O}_3$ nanoparticles, bare graphitic carbon, physically mixed $\alpha\text{-Fe}_2\text{O}_3\text{/graphite}$, and $\alpha\text{-Fe}_2\text{O}_3\text{@GC}$ at 400 mA g^{-1} (b), representative charge-discharge profiles at various current densities (c), and rate performance (d) of $\alpha\text{-Fe}_2\text{O}_3\text{@GC}$. $1\text{ C} = 1000\text{ mA g}^{-1}$.

electrochemical performance of pure graphitic carbon microspheres obtained by eliminating $\alpha\text{-Fe}_2\text{O}_3$ from the $\alpha\text{-Fe}_2\text{O}_3\text{@GC}$ was also tested (Fig. S5). The pure graphitic carbon spheres show an irreversible capacity of 670 mA h g^{-1} in the first cycle. Considering the carbon content (27 %) of the $\alpha\text{-Fe}_2\text{O}_3\text{@GC}$ composite, the graphitic carbon would contribute a high irreversible capacity of 181 mA h g^{-1} to the $\alpha\text{-Fe}_2\text{O}_3\text{@GC}$ composite in the first discharge-charge process. The initial Coulombic efficiency of $\alpha\text{-Fe}_2\text{O}_3\text{@GC}$ can be improved from 66 % to 85.5 % by applying a prelithiation strategy (Fig. S6).⁴⁰ In the subsequent cycles, the Coulombic efficiency increases dramatically to 96 % and levels off at 97–100 % onwards. The cycling performance of $\alpha\text{-Fe}_2\text{O}_3\text{@GC}$ is presented in Fig. 4b. A high capacity as high as 841 mA h g^{-1} is still maintained even after 100 cycles, suggesting the excellent cycling stability. For the purpose of comparison, the electrochemical properties of pristine $\alpha\text{-Fe}_2\text{O}_3$ nanoparticles and bare graphitic carbon spheres were also studied. The $\alpha\text{-Fe}_2\text{O}_3$ nanoparticles with sizes of 25–50 nm (Fig. S7) show an initial discharge capacity of 1023 mA h g^{-1} , fading to 223 mA h g^{-1} after 100 cycles. The pure graphitic carbon spheres exhibit a relatively low reversible capacity of approximately 370 mA h g^{-1} with outstanding cycling stability. Physically mixed $\alpha\text{-Fe}_2\text{O}_3\text{/graphite}$ shows fast capacity fading under the same test conditions. A capacity of 140 mA h g^{-1} is retained after 100 cycles (Fig. 4b). These results ambiguously demonstrate that the graphitic carbon not only contributes to the Li storage capacity but also plays a

crucial role in enhancing the structural stability and thus the cycling stability of the electrode.

The rate performance of $\alpha\text{-Fe}_2\text{O}_3\text{@GC}$ was further investigated at various current densities ranging from 0.4 to 6 C (Fig. 4c, 4d). A high capacity of 880 mA h g^{-1} is achieved at 0.4 C. The capacity decreases slightly with the stepwise increase of current density. Even at a high current density of 6 C, a capacity of 350 mA h g^{-1} is still retained. Remarkably, a stable capacity of 860 mA h g^{-1} can be resumed when the current is reduced to 0.4 C, which remains 97.7 % of the initial capacity before high rate test. Such an excellent electrochemical performance in terms of cycling stability and rate capability is superior to or at least comparable with those of state-of-the-art $\alpha\text{-Fe}_2\text{O}_3$ based anode materials in previous reports (Table S1).

The high reversible capacity, excellent cycling stability, and outstanding rate capability can be attributed to the unique structure of $\alpha\text{-Fe}_2\text{O}_3\text{@GC}$. In the constructed composite, the $\alpha\text{-Fe}_2\text{O}_3$ nanoparticles act as the primary active material, providing high capacity. Considering the weight percentage of $\alpha\text{-Fe}_2\text{O}_3$ in the composite, it can contribute 735 mA h g^{-1} ($1007\text{ mA h g}^{-1} \times 73\%$) to the total capacity. The nanocrystalline characteristic of $\alpha\text{-Fe}_2\text{O}_3$ greatly shortens the diffusion lengths for both electrons and lithium ions, contributing to the high rate capability. Meanwhile, the graphitic carbon shells serve four main purposes. I) They act as the secondary active component, contributing to the total capacity of the composite. Assuming a capacity of 372 mA h g^{-1} for graphitic carbon, the graphitic

carbon in the α -Fe₂O₃@GC could contribute 100 mA h g⁻¹ (372 mA h g⁻¹ × 27%) to the total capacity. II) The graphitic carbon shells serve as the structural stabilizer, effectively buffering the large volume change, inhibiting the aggregation, and preventing the pulverization of α -Fe₂O₃. To demonstrate the structural stability, the morphology of the active material before and after 100 cycles at 400 mA g⁻¹ was checked by SEM. As shown in Fig. S8, the original microspherical morphology of α -Fe₂O₃@GC can be well maintained. Bearing the structural integrity in mind, it is not surprising that the α -Fe₂O₃@GC shows significantly improved cycling stability than pristine α -Fe₂O₃ nanoparticles and physically mixed α -Fe₂O₃/graphite (Fig. 4b). III) The graphitic carbon shells serve as the interfacial stabilizer, preventing the direct exposure of α -Fe₂O₃ nanoparticles to the electrolyte, and thus resulting in a stable electrode-electrolyte interphase.^{32, 41} IV) The graphitic carbon matrix wires the whole composite, acting as a highway for electron transport, and thus significantly enhancing the rate capability.

Conclusion

In summary, a novel "spray drying-carbonization-oxidation" strategy has been developed for the fabrication of α -Fe₂O₃@GC nanocomposite. With the α -Fe₂O₃ nanoparticles well-encapsulated in onion-like graphitic carbon shells, the resulting α -Fe₂O₃@GC exhibits remarkable electrochemical performance. A reversible capacity as high as 898 mA h g⁻¹ can be achieved at 400 mA g⁻¹, maintaining 841 mA h g⁻¹ after 100 cycles. Our product, in terms of the facile and scalable preparation process and excellent electrochemical performance, demonstrates its great potential as a LIBs anode. It is also expected that this strategy could be extended to the fabrication of other transition metal oxide-graphitic carbon nanocomposites such as Co_xO_y@GC, NiO@GC, and Mn_xO_y@GC.

Acknowledgements

The authors acknowledge the Australian Research Council and the Queensland Government for the financial support, the Australian National Fabrication Facility and the Australian Microscopy and Microanalysis Research Facility at the Centre for Microscopy and Microanalysis, The University of Queensland for technical supports. L. Z. gratefully acknowledges the award of UQ Postdoctoral Research Fellowship and UQ Foundation Research Excellence Awards.

Notes and references

^a Australian Institute for Bioengineering and Nanotechnology, The University of Queensland, Brisbane, QLD 4072, Australia

E-mail: l.zhou1@uq.edu.au

† Electronic Supplementary Information (ESI) available: XRD pattern, XPS spectrum, CV curves, TEM and SEM images, and table. See DOI: 10.1039/b000000x/

- J. M. Tarascon and M. Armand, *Nature*, 2001, **414**, 359-367.
- M. Armand and J. M. Tarascon, *Nature*, 2008, **451**, 652-657.
- P. Poizot, S. Laruelle, S. Grugeon, L. Dupont and J. M. Tarascon, *Nature*, 2000, **407**, 496-499.
- M. V. Reddy, G. V. S. Rao and B. V. R. Chowdari, *Chem. Rev.*, 2013, **113**, 5364-5457.
- J. Chen, L. N. Xu, W. Y. Li and X. L. Gou, *Adv. Mater.*, 2005, **17**, 582-586.
- N. Kang, J. H. Park, J. Choi, J. Jin, J. Chun, I. G. Jung, J. Jeong, J. G. Park, S. M. Lee, H. J. Kim and S. U. Son, *Angew. Chem. Int. Ed.*, 2012, **51**, 6626-6630.
- Z. Y. Wang, D. Y. Luan, S. Madhavi, C. M. Li and X. W. Lou, *Chem. Commun.*, 2011, **47**, 8061-8063.
- J. P. Liu, Y. Y. Li, H. J. Fan, Z. H. Zhu, J. Jiang, R. M. Ding, Y. Y. Hu and X. T. Huang, *Chem. Mater.*, 2010, **22**, 212-217.
- Y. M. Lin, P. R. Abel, A. Heller and C. B. Mullins, *J. Phys. Chem. Lett.*, 2011, **2**, 2885-2891.
- H. Liu, G. X. Wang, J. Park, J. Wang, H. Liu and C. Zhang, *Electrochim. Acta*, 2009, **54**, 1733-1736.
- C. T. Cheria, J. Sundaramurthy, M. Kalaivani, P. Ragupathy, P. S. Kumar, V. Thavasi, M. V. Reddy, C. H. Sow, S. G. Mhaisalkar, S. Ramakrishna and B. V. R. Chowdari, *J. Mater. Chem.*, 2012, **22**, 12198-12204.
- X. Y. Yao, C. L. Tang, G. X. Yuan, P. Cui, X. X. Xu and Z. P. Liu, *Electrochem. Commun.*, 2011, **13**, 1439-1442.
- M. V. Reddy, T. Yu, C. H. Sow, Z. X. Shen, C. T. Lim, G. V. S. Rao and B. V. R. Chowdari, *Adv. Funct. Mater.*, 2007, **17**, 2792-2799.
- Y. H. Xu, G. Q. Jian, Y. H. Liu, Y. J. Zhu, M. R. Zachariah and C. S. Wang, *Nano Energy*, 2014, **3**, 26-35.
- X. Xu, R. Cao, S. Jeong and J. Cho, *Nano Lett.*, 2012, **12**, 4988-4991.
- B. Wang, J. S. Chen, H. B. Wu, Z. Y. Wang and X. W. Lou, *J. Am. Chem. Soc.*, 2011, **133**, 17146-17148.
- L. Zhang, H. B. Wu, S. Madhavi, H. H. Hng and X. W. Lou, *J. Am. Chem. Soc.*, 2012, **134**, 17388-17391.
- L. Zhou, H. Y. Xu, H. W. Zhang, J. Yang, S. B. Hartono, K. Qian, J. Zou and C. Z. Yu, *Chem. Commun.*, 2013, **49**, 8695-8697.
- S. M. Xu, C. M. Hessel, H. Ren, R. B. Yu, Q. Jin, M. Yang, H. J. Zhao and D. Wang, *Energy Environ. Sci.*, 2014, **7**, 632-637.
- M. Y. Son, Y. J. Hong, J. K. Lee and Y. C. Kang, *Nanoscale*, 2013, **5**, 11592-11597.
- J. M. Jeong, B. G. Choi, S. C. Lee, K. G. Lee, S. J. Chang, Y. K. Han, Y. B. Lee, H. U. Lee, S. Kwon, G. Lee, C. S. Lee and Y. S. Huh, *Adv. Mater.*, 2013, **25**, 6250-6255.
- S. L. Chou, J. Z. Wang, D. Wexler, K. Konstantinov, C. Zhong, H. K. Liu and S. X. Dou, *J. Mater. Chem.*, 2010, **20**, 2092-2098.
- X. J. Zhu, Y. W. Zhu, S. Murali, M. D. Stollers and R. S. Ruoff, *ACS Nano*, 2011, **5**, 3333-3338.
- H. W. Zhang, L. Zhou and C. Z. Yu, *RSC Adv.*, 2014, **4**, 495-499.
- W. J. Yu, P. X. Hou, L. L. Zhang, F. Li, C. Liu and H. M. Cheng, *Chem. Commun.*, 2010, **46**, 8576-8578.
- Z. Y. Wang, D. Y. Luan, S. Madhavi, Y. Hu and X. W. Lou, *Energy Environ. Sci.*, 2012, **5**, 5252-5256.
- G. M. Zhou, D. W. Wang, P. X. Hou, W. S. Li, N. Li, C. Liu, F. Li and H. M. Cheng, *J. Mater. Chem.*, 2012, **22**, 17942-17946.
- W. J. Lee, T. H. Hwang, J. O. Hwang, H. W. Kim, J. Lim, H. Y. Jeong, J. Shim, T. H. Han, J. Y. Kim, J. W. Choi and S. O. Kim, *Energy Environ. Sci.*, 2014, **7**, 621-626.
- W. J. Lee, J. M. Lee, S. T. Kochuveedu, T. H. Han, H. Y. Jeong, M. Park, J. M. Yun, J. Kwon, K. No, D. H. Kim and S. O. Kim, *ACS Nano*, 2012, **6**, 935-943.
- L. Chen, Z. Y. Wang, C. N. He, N. Q. Zhao, C. S. Shi, E. Z. Liu and J. J. Li, *ACS Appl. Mater. Interfaces*, 2013, **5**, 9537-9545.
- L. Zhang, M. J. Zhang, Y. H. Wang, Z. L. Zhang, G. W. Kan, C. G. Wang, Z. Y. Zhong and F. B. Su, *J. Mater. Chem. A*, 2014, **2**, 10161-10168.
- C. N. He, S. Wu, N. Q. Zhao, C. S. Shi, E. Z. Liu and J. J. Li, *ACS Nano*, 2013, **7**, 4459-4469.
- M. C. Mangarella, J. L. Ewbank, M. R. Dutzer, F. M. Alamgir and K. S. Walton, *Carbon*, 2014, **79**, 74-84.
- M. Sevilla, C. Sanchis, T. Valdes-Solis, E. Morallon and A. B. Fuertes, *Carbon*, 2008, **46**, 931-939.
- H. W. Zhang, L. Zhou, O. Noonan, D. J. Martin, A. K. Whittaker and C. Z. Yu, *Adv. Funct. Mater.*, 2014, **24**, 4337-4342.
- N. Liu, Z. D. Lu, J. Zhao, M. T. McDowell, H. W. Lee, W. T. Zhao and Y. Cui, *Nat. Nanotechnol.*, 2014, **9**, 187-192.
- J. Y. Wang, N. L. Yang, H. J. Tang, Z. H. Dong, Q. Jin, M. Yang, D. Kisailus, H. J. Zhao, Z. Y. Tang and D. Wang, *Angew. Chem. Int. Ed.*, 2013, **52**, 6417-6420.
- G. M. Zhou, D. W. Wang, F. Li, L. L. Zhang, N. Li, Z. S. Wu, L. Wen, G. Q. Lu and H. M. Cheng, *Chem. Mater.*, 2010, **22**, 5306-5313.

- 39 J. X. Wang, W. Li, F. Wang, Y. Y. Xia, A. M. Asiri and D. Y. Zhao, *Nanoscale*, 2014, **6**, 3217-3222.
- 40 C. R. Jarvis, M. J. Lain, M. V. Yakovleva and Y. Gao, *J. Power Sources*, 2006, **162**, 800-802.
- 41 H. Wu, G. Chan, J. W. Choi, I. Ryu, Y. Yao, M. T. McDowell, S. W. Lee, A. Jackson, Y. Yang, L. B. Hu and Y. Cui, *Nat. Nanotechnol.*, 2012, **7**, 309-314